Engineering Structures 343 (2025) 121249

Contents lists available at ScienceDirect

Engineering Structures

journal homepage: www.elsevier.com/locate/engstruct

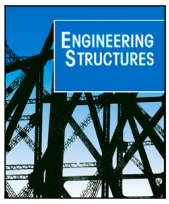

An engineering approach to evaluate stress concentrations at openings in CLT shear walls☆

Markus Detter *, Georg Hochreiner, Josef Füssl

Institute for Mechanics of Materials and Structures, TU Wien, Karlsplatz 13, Vienna, 1040, Austria

ARTICLE INFO

Keywords:
Mass timber
Cross-laminated timber (CLT)
Linear elastic fracture mechanics (LEFM)
Finite element method (FEM)

ABSTRACT

In the past decade, the construction of mass timber buildings made from sustainable cross-laminated timber (CLT) has increased significantly. However, openings such as doors or windows in CLT shear walls can substantially reduce their load-bearing capacity. Many design standards address this by neglecting wall segments with openings, leading to inefficient designs and inaccurate internal force distributions in CLT buildings. While current design standards provide guidance for wall sections without openings, they lack suitable approaches for geometries with discontinuities, where stress concentrations occur. To address this gap, we propose a fracture mechanics-based method to predict brittle failure at corners using 2D linear elastic finite element (FE) models. The method evaluates Mode I and Mode II energy release rates based on mean stresses and applies a mixed-mode fracture criterion. The modeling framework accounts for orthotropic material behavior, local mesh refinement around singularities, and nonlinear connection behavior. The models are validated against published experimental data, and the results show good agreement for both crack-driven and connection-driven failure cases. A sensitivity analysis with respect to key parameters influencing the total energy release rate confirms the robustness of the proposed approach. These findings support the method's applicability for practical design purposes and pave the way for its broader use in other timber engineering applications.

1. Introduction

In the last decade, the worldwide production of cross-laminated timber (CLT) has increased significantly. For example, the annual European production of CLT nearly doubled from 2015 to 2020, reaching 1.2 million m^3 [1]. As of now, there is no indication that this remarkable growth will slow down, owing to various factors. Firstly, the main reason is the building sector's pursuit of green, sustainable, and CO_2-reducing construction methods. Mass timber buildings made from CLT meet these objectives. Secondly, CLT buildings exhibit excellent performance in response to natural hazards such as earthquakes, showing no disadvantages compared to traditional construction methods. CLT structures demonstrate robust seismic behavior, which allows for the construction of mid- and high-rise buildings even in regions prone to high seismic activity [2,3]. Thirdly, CLT elements can be prefabricated to various extents, resulting in reduced assembly times and rapid construction progress.

Mass timber buildings constructed from CLT primarily consist of two structural CLT components: ceilings and walls. Walls in these structures serve dual load-bearing roles. They support vertical forces resulting from dead loads, live loads, and others, and they also withstand horizontal forces generated by wind and earthquakes. The impact of these horizontal loads intensifies with the increase in building height. To effectively channel these forces from each storey into the foundation, the use of so-called shear walls is essential.

In shear walls, two primary failure mechanisms can be observed in experiments, both of which determine the load-bearing capacity [4,5]. Either the anchors at the base of the wall, such as hold-downs and angle brackets, fail, or the wall itself fails. In some cases, both failure mechanisms occur simultaneously, depending on the specific arrangement and properties of the connectors, the geometry of the wall, and the load configuration. Therefore, the failure of a CLT wall is a rather complex process.

When openings in walls, mainly windows and doors, are required, two fabrication options are possible [2,4]. In a monolithic wall, openings are cut out on the CNC production line from a whole CLT plate. Alternatively, a segmented wall is constructed from several smaller panels, including areas without openings, lintels, and parapets, which are assembled to form the entire wall.

☆ This article is part of a Special issue entitled: 'Mass Timber Systems' published in Engineering Structures.

* Corresponding author.
E-mail address: markus.detter@tuwien.ac.at (M. Detter).

https://doi.org/10.1016/j.engstruct.2025.121249

Available online 4 September 2025

In the structural design process, it is important to distinguish between monolithic CLT walls without openings, monolithic CLT walls with openings, and segmented CLT walls with openings, due to their differing mechanical behaviors. Additionally, the arrangement and specific mechanical properties of the connectors should be incorporated into the design process. Finite element software is a very good and efficient way to plausibly model those mechanisms. The structural behavior, as well as the influence of geometry and boundary conditions, can be modeled in a highly realistic and straightforward manner. However, stress concentrations that occur in the corner areas of openings are often critical for design purposes and must be interpreted appropriately. Particularly in linear elastic analysis, which is very common in engineering, stress singularities arise and are often misjudged.

1.1. State of the art and previous research

Although there are mechanical differences between monolithic and segmented walls, both are often treated similarly in the structural design process by civil engineers. This approach usually considers only the wall areas without lintels and parapets for the horizontal load-bearing capacity, resulting in each wall element acting as an independent vertical cantilever. However, this simplification can lead to an underestimation of the shear resistance in buildings with CLT walls [2,6]. Both types of walls also exhibit significantly different horizontal stiffness. Inaccurate modeling, therefore, results in unrealistic force distributions in the building model. So, from various points of view, both construction methods should not be treated similarly in the modeling of CLT buildings.

Several studies related to CLT walls with openings have been conducted over the past two decades. Dujic et al. [6], based on a parametric study, demonstrated that the load-bearing capacity of CLT walls with openings up to 30 % of the total area is not significantly affected, although the stiffness in such cases is reduced by approximately 50 %. Shahnewaz et al. [7] studied the influence of openings on wall stiffness using finite element modeling. They conducted a parametric study by varying the size and shape of the openings, the aspect ratios of the openings, and the aspect ratios of the walls. Mestar et al. [4] investigated the kinematic behavior of CLT shear walls with openings using full-scale tests and numerical models. The study found that the slenderness of the lintel and the stiffness of the hold-downs significantly influence the kinematic behavior. Casagrande et al. [5] conducted both experimental and numerical studies on the mechanical behavior of CLT shear walls with openings to identify failure modes and proposed a numerical procedure to predict the load-bearing capacity. In this study, 2D finite element simulations were used, with areas near stress singularities excluded from the verification. The recommendations for these exclusion zones are based on the findings of Casagrande et al. [2], where a parametric study using finite element software was conducted to explore the distribution of internal forces in single-story CLT shear walls with openings. Sciomenta [8] demonstrated how to simulate CLT walls with openings using the extended finite element method (XFEM) and validated her model against experimental results from [5]. Isoda et al. [9] conducted experiments to investigate the behavior of L-shaped and T-shaped CLT elements for the evaluation of shear walls with openings. D'Arenzo [10] presented an analytical model to predict the lateral response of CLT shear walls with openings.

In most cases of the simulations, either stress singularities were deliberately excluded in the verifications or advanced simulation methods were employed to directly address them. Unfortunately, such advanced methods, like XFEM, are not available in commercial FE software commonly used by civil engineers in practice. Highly nonlinear simulations would also be too complex for the typical verification process.

1.2. Scope of this paper

Current design standards lack specific guidance on how to verify geometrical arbitrary CLT walls with openings. Furthermore, there are no official guidelines for modeling CLT shear members in finite element software or for addressing resulting stress singularities. Thus, the need for a standardized procedure to address these issues is evident. In this paper, we demonstrate how to model CLT walls with openings using 2D finite element simulations with orthotropic material behavior and propose a novel universally applicable approach to assess stress concentrations at openings of CLT shear walls. A simple and as universal as possible applicability of this approach was a requirement of our defined research question, so that civil engineers in practice can handle stress singularities in FE simulations straightforwardly.

In Section 2, we present the theoretical background for applying fracture mechanics to 2D finite element models of CLT shear members. This section also introduces our proposed approach for addressing stress singularities and discusses experimental campaigns found in the literature that validate our approach. In Section 3, the numerical models of the experiments, which are used for validation, are described in detail. In Section 4, we present the results of these numerical models and compare them with the experimental outcomes. In Section 5, we give our conclusions and discuss the potential applications of the proposed approach to other mechanical problems.

2. Materials and methods

This chapter is divided into four parts. First, we present in Section 2.1 the theoretical background and the foundation of our proposed approach to assess stress singularities in CLT members, which is shown in Section 2.2. Subsequently, we demonstrate how to model CLT members using 2D finite elements, as detailed in Section 2.3. Finally, in Section 2.4, we describe the various experimental campaigns used to validate our approach.

2.1. Theoretical backround – LEFM

In linear-elastic finite element simulations using 2D elements, stress singularities typically occur at the corners of rectangular openings. Theoretically, the stress at these corners increases to infinity, making the use of stress-based verification criteria for this situation inapplicable. Fracture mechanics, particularly linear elastic fracture mechanics (LEFM), offers a robust approach to address these singularities. LEFM is especially valuable for validating stress concentrations without significantly increasing the computational time of finite element models, thereby maintaining practical feasibility.

There are various approaches to implementing LEFM for validation, such as the compliance method, stress-intensity factors, the mean stress method, and others. LEFM is a theory based on the assumptions that the material behaves in a linearly elastic manner, that the fracture process zone (FPZ) is small compared to the characteristic dimensions of the structure, and that a stress singularity exists. Wood loaded perpendicularly to the grain in tension (Mode I) and shear (Mode II) exhibits nearly linear elastic and quasi-brittle fracture behavior, characterized by a small nonlinear region before the peak stress and progressive softening in the post-peak behavior. Additionally, CLT members used in standard building applications are relatively large; therefore, we assume that the geometric requirements for the FPZ are satisfied.

Since the critical energy release rates $G_{\mathrm{I,c}}$ for Mode I and $G_{\mathrm{II,c}}$ for Mode II – which in LEFM are equal to the fracture energies – are known material parameters for commonly used wood species, we can assess the validity of our assumptions in this context and determine whether LEFM is applicable and capable of predicting elastic limits of CLT shear walls with openings.

For our proposed approach, we adapted the so-called *mean stress method*, originally derived by Gustafsson in [11]. With this adaptation,

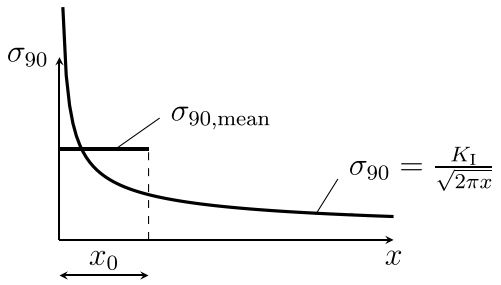

Fig. 1. Qualitative representation of the stress distribution σ_{90} at a crack tip and the corresponding mean stress $\sigma_{90,\text{mean}}$.

it is possible to calculate the energy release rates G_I and G_II at stress singularities using the resulting mean stresses $\sigma_{90,\text{mean}}$ (stress perpendicular to the grain) and $\tau_{090,\text{mean}}$ (membrane shear stress) obtained from a single 2D linear-elastic finite element analysis. In the following, the derivation of this method is presented. The direction parallel to the fiber is defined as 0, and the direction normal to the fiber is defined as 90.

In the vicinity of a crack tip, under the assumptions of LEFM, a so-called $1/\sqrt{r}$ singularity of stresses and strains occurs, where r represents the radius as the distance from the crack tip. An example of this analytical stress distribution is shown in Fig. 1 for tensile stress σ_{90} perpendicular to the grain. Here, x denotes the horizontal distance from the crack tip. At the crack tip, the stresses approach infinity. Typically, for solid timber, the potential crack surface follows the fiber direction.

To solve the problem of the infinite stresses, Irwin [12] developed the concept of stress intensity factors, known as K-factors. These factors allow for the description of stress fields in the vicinity of a crack tip along the potential crack surface. The transverse tensile stresses σ_{90} and shear stresses τ_{090} can then be calculated using the stress intensity factors K_I for Mode I and K_II for Mode II, as follows:

$$\sigma_{90} = \frac{K_\text{I}}{\sqrt{2\pi x}}\,, \tag{1}$$

$$\tau_{090} = \frac{K_\text{II}}{\sqrt{2\pi x}}\,. \tag{2}$$

If the potential crack follows the principal material directions of an orthotropic material, which is typically the case for wood, the relationships between the energy release rates G_I and G_II and the stress intensity factors K_I and K_II, as described by Gustafsson in [11], are given by:

$$G_\text{I} = \frac{K_\text{I}^2}{E_\text{I}}\,, \tag{3}$$

$$G_\text{II} = \frac{K_\text{II}^2}{E_\text{II}}\,, \tag{4}$$

where E_I and E_II are defined as follows:

$$\frac{1}{E_\text{I}} = \frac{1}{E_0}\sqrt{\frac{E_0}{2E_{90}}}\sqrt{\sqrt{\frac{E_0}{E_{90}}} + \frac{E_0}{2G_{090}} - \nu_{900}\frac{E_0}{E_{90}}}\,, \tag{5}$$

$$\frac{1}{E_\text{II}} = \frac{1}{E_0}\sqrt{\frac{1}{2}}\sqrt{\sqrt{\frac{E_0}{E_{90}}} + \frac{E_0}{2G_{090}} - \nu_{900}\frac{E_0}{E_{90}}}\,. \tag{6}$$

Here, E_0 and E_{90} represent Young's moduli in the corresponding material directions, with the fiber direction aligned along the 0-axis. G_{090} is the shear modulus, and ν_{900} is the Poisson's ratio.

Using Eqs. (1) and (2), the mean stresses $\sigma_{90,\text{mean}}$ and $\tau_{090,\text{mean}}$ over a length x_0 can be calculated as follows:

$$\sigma_{90,\text{mean}} = \frac{1}{x_0}\int_0^{x_0}\frac{K_\text{I}}{\sqrt{2\pi x}}dx = \sqrt{\frac{2K_\text{I}^2}{\pi x_0}}\,, \tag{7}$$

$$\tau_{090,\text{mean}} = \frac{1}{x_0}\int_0^{x_0}\frac{K_\text{II}}{\sqrt{2\pi x}}dx = \sqrt{\frac{2K_\text{II}^2}{\pi x_0}}\,. \tag{8}$$

For example, $\sigma_{90,\text{mean}}$ is illustrated in Fig. 1. Using the mean stresses from Eqs. (7) and (8), Gustafsson proposed the so-called *mean stress approach* in [11], where fracture is described using a stress-based failure criterion. Serrano further demonstrated applications of this method in [13,14].

By rearranging Eqs. (7) and (8) to express K_I and K_II, and substituting them into Eqs. (3) and (4), we obtain:

$$G_\text{I} = \frac{\sigma_{90,\text{mean}}^2\pi x_0}{2E_\text{I}}\,, \tag{9}$$

$$G_\text{II} = \frac{\tau_{090,\text{mean}}^2\pi x_0}{2E_\text{II}}\,. \tag{10}$$

Thus, with Eqs. (9) and (10), it is possible to obtain the energy release rates G_I and G_II using the mean stresses $\sigma_{90,\text{mean}}$ and $\tau_{090,\text{mean}}$, which can be derived from a 2D finite element analysis. The length x_0 has no impact as long as the stress distributions precisely follow Eqs. (1) and (2).

This differs from that proposed by Gustafsson in [11]. There, to achieve equivalent results using stress intensity factors K, it is necessary to calculate x_0 based on material parameters such as Young's moduli, shear modulus, fracture energies, tensile strength, and shear strength. The calculation of x_0 also depends on the resulting mixed-mode ratio $k = K_\text{II}/K_\text{I}$, which is determined through an iterative process. Typical values for x_0 for pure Mode I in solid softwood range between 10 mm and 30 mm [11,15,16].

Since in our approach x_0 is independent of material properties and the mixed-mode ratio, we used a fixed value of $x_0 = 15$ mm for all calculations. Notably, this value also corresponds to the result obtained for pure Mode I fracture using the formulation in [11] including the stiffness parameters shown in Fig. A.12, a critical energy release rate of $G_{\text{I},c} = 300\,\text{N/m}$, and a tensile strength perpendicular to the grain of $f_{\text{t},90} = 3\,\text{N/mm}^2$. In the Appendix, we show that the value of x_0 has no significant influence on the results when analyzing a notch using the proposed approach.

Finally, we propose to apply the obtained energy release rates G_I and G_II to the fracture criterion $f(\mathbf{G})$, presented by Wu [17], which is expressed in energy terms as follows:

$$f(\mathbf{G}) = \sqrt{\frac{G_\text{I}}{G_{\text{I,c}}} + \frac{G_\text{II}}{G_{\text{II,c}}}} = 1.0\,. \tag{11}$$

Here, $G_{\text{I,c}}$ is the critical energy release rate perpendicular to the grain (Mode I), and $G_{\text{II,c}}$ is the critical energy release rate for shear (Mode II).

2.2. Application of the proposed approach

In CLT, the potential crack directions at corners can typically be defined in advance. Cracks that initiate in corners generally follow the wood fiber direction, at least at the beginning of the crack progression and, therefore, in the stage relevant for a conservative verification procedure. This behavior was observed in the experiments by Casagrande et al. [5], Mestar et al. [4], Aljuhmani et al. [18], and Gschwendtner [19].

For example, Fig. 2 illustrates a three-layered CLT wall panel with a door opening, showing potential cracks in both the inner and outer layers at the left corner. By modeling this CLT wall panel using 2D linear-elastic finite elements, which is described in Section 2.3, we can determine the stresses in the potential crack directions for each layer, which include tensile stresses perpendicular to the local grain direction σ_{90} and membrane shear stresses τ_{090}. These stresses are also qualitatively depicted in Fig. 2 for both the inner and outer layers.

Knowing these stress distributions, it is possible to calculate the mean stresses $\sigma_{90,\text{mean}}$ and $\tau_{090,\text{mean}}$ for each layer i of N layers of the

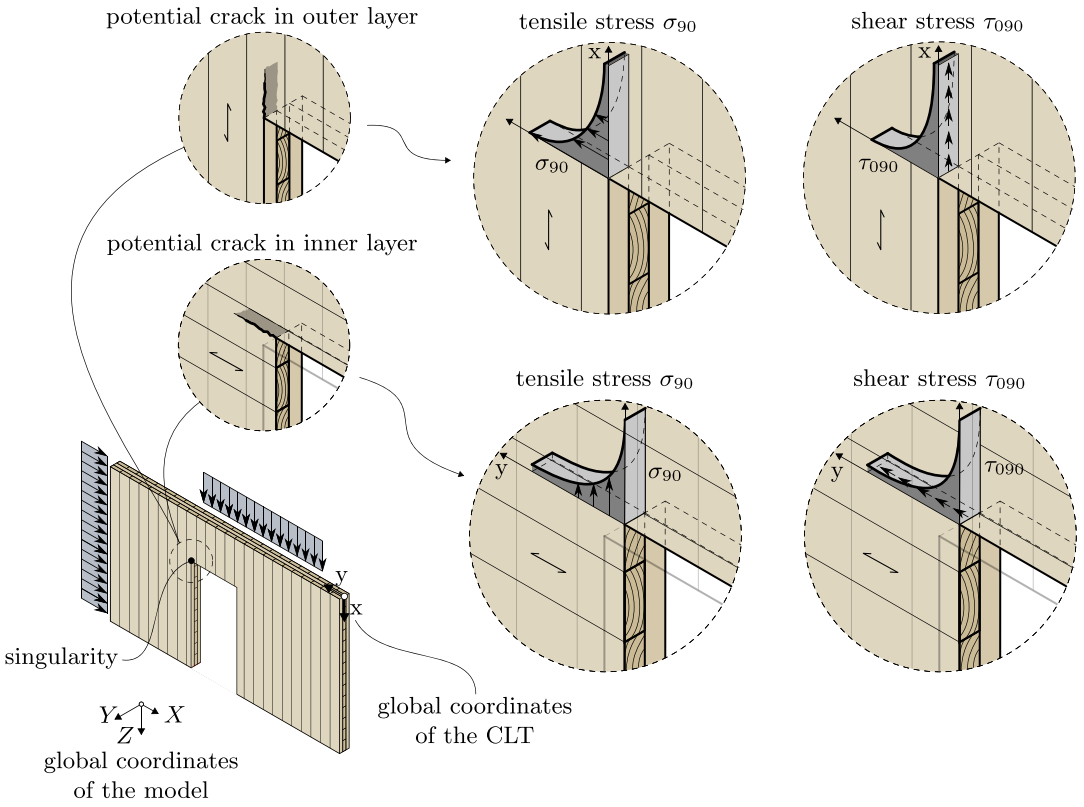

Fig. 2. Potential crack formation in a CLT wall panel with a door opening and corresponding linear elastic stress distributions.

CLT panel. Further, the energy release rates can be calculated according to Eqs. (9) and (10) for each layer i at the corner. These calculations enable the use of the fracture criterion in Eq. (11) to predict whether a crack will develop.

For predicting the load-bearing capacity of the entire CLT corner, we present two failure criteria. The first and also the more conservative approach calculates an elastic limit, which is reached if a crack occurs in at least one layer i out of N layers, mathematically expressed (with the operator OR) as:

$$\bigvee_{i=1}^{N} f(\mathbf{G})_i \geq 1 \ . \tag{12}$$

The second, less conservative approach, assumes that failure of the corner occurs only if cracks develop in all layers, mathematically expressed (with the operator AND) as:

$$\bigwedge_{i=1}^{N} f(\mathbf{G})_i \geq 1 \quad \text{which means} \quad \forall i \in \{1, 2, \dots, N\} : f(\mathbf{G})_i \geq 1 \ . \tag{13}$$

2.3. Modeling of CLT using 2D finite elements

In our FE models, we utilized 2D shell elements with orthotropic stiffness properties. The calculations were performed using the FE software RFEM 5 [20], which is commonly used by engineers in the building design process. First, we show in Section 2.3.1 how to calculate the stiffness properties for a CLT member, and second, the calculation of stresses acting in the layers is shown in Section 2.3.2.

2.3.1. Stiffness properties of CLT

CLT can be mechanically described using classical laminate theory. Details on classical laminate theory can be found, for example, in Jones [21]. Fig. 3 illustrates a symmetric laminate consisting of N layers, with each layer defined by z-coordinates, which are referenced to the middle surface.

In the case of CLT, simplifications are made: Neglecting the Poisson's ratios ν_{xy} and ν_{yx} is justified based on the structure of the element made from individual boards and the formation of gaps or cracks parallel to the boards, as explained by Wallner-Novak et al. [22]. Additionally, Bogensperger and Silly [23] also states that CLT members are not joint-free and crack-free continuums.

Since we are modeling plane problems with in-plane-loading, only two membrane stiffnesses (S_{xx} and S_{yy}) and one membrane shear stiffness (S_{yx}) need to be calculated.

By neglecting the Poisson ratios ν_{xy} and ν_{yx}, the determination of the membrane stiffnesses is conducted as follows:

$$S_{xx} = \sum_{k=1}^{N} E_{x,k}(z_k - z_{k-1}) \ , \tag{14}$$

$$S_{yy} = \sum_{k=1}^{N} E_{y,k}(z_k - z_{k-1}) \ , \tag{15}$$

where $E_{x,k}$ and $E_{y,k}$ are the Young's modulus of the layers in x- and y-direction of the CLT member.

The shear stiffness of a CLT panel per length unit, S_{xy}, is determined according to the Austrian National Annex of Eurocode 5 (EC5) [24]. The equation is as follows:

$$S_{xy} = \frac{G_{0,\text{mean}} t}{1 + 6 p_S \left(\frac{t_{max}}{a}\right)^{q_S}} \ , \tag{16}$$

where t is the thickness of the CLT member, and t_{max} is the thickness of the thickest layer. The width of the boards is denoted by a. The parameters p_S and q_S are dependent on the number of layers and can be taken from the Austrian National Annex of EC5 [24].

The constitutive relation between the membrane forces and the membrane strains can be stated as:

$$\begin{bmatrix} n_x \\ n_y \\ n_{xy} \end{bmatrix} = \begin{bmatrix} S_{xx} & 0 & 0 \\ 0 & S_{yy} & 0 \\ 0 & 0 & S_{xy} \end{bmatrix} \cdot \begin{bmatrix} \varepsilon_x \\ \varepsilon_y \\ \gamma_{xy} \end{bmatrix} \ . \tag{17}$$

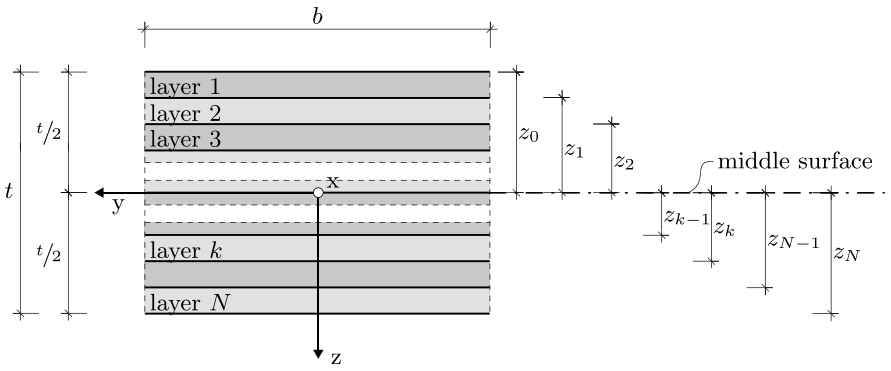

Fig. 3. Notations for a laminate member comprising N layers as described in [21].

2.3.2. Stress distribution in CLT

The longitudinal stress $\sigma_{x,k}$ and the transverse stress $\sigma_{y,k}$ in each layer k, both in reference to the global coordinate system of the CLT member, are calculated according to classical laminate theory as follows:

$$\sigma_{x,k} = E_{x,k}\left(\frac{n_x}{S_{xx}}\right) , \tag{18}$$

$$\sigma_{y,k} = E_{y,k}\left(\frac{n_y}{S_{yy}}\right) . \tag{19}$$

with the normal forces n_x and n_y. For analyzing each layer, these stresses (Eqs. (18) and (19)) have to be converted into the local coordinate system of each layer k, resulting in $\sigma_{0,k}$ and $\sigma_{90,k}$, where "0" is parallel to the grain direction and "90" denotes the direction perpendicular to grain. For the further calculation of the corresponding energy release rate in Mode I, only $\sigma_{90,k}$ is required.

The shear stress τ_{xy} respectively τ_{yx} (related to the gross cross-section) due to shear force n_{xy} respectively n_{yx} in CLT is calculated as follows:

$$\tau_{xy} = \tau_{yx} = \tau_{090} = \tau_{900} = \frac{n_{xy}}{t} = \frac{n_{yx}}{t} . \tag{20}$$

Here, it is not necessary to perform a coordinate transformation between the global coordinate system of the entire CLT member and the local coordinate systems specific to each layer.

Depending on the CLT producer, the boards within a layer can be edge-glued or not edge-glued. If a CLT member is made out of not edge-glued boards, the transverse stiffness of the boards E_{90} is set to zero, so, therefore, no transverse stresses σ_{90} can occur. In the design of CLT members, this is commonly also implemented for edge-glued boards as stated in Bogensperger and Silly [23]. The reason here is the possibility of shrinkage-induced cracks and, therefore gaps in the fiber direction between and in the boards so that no stress transmission is possible. Based on this assumption, just longitudinal stresses are accounted for in the verification, which also makes the design process easier.

To apply our proposed approach for evaluating stress concentrations at openings, we must deviate from this commonly used procedure. Therefore, we define two regions in a CLT wall: First, the regular region (reg-region) without stress singularities, and second, detailed regions with singularities (sin-region), for example, at corners. Both regions should be modeled in the FE software with the same stiffness properties, however, a crucial distinction is made for the calculation of the occurring stresses.

In the vicinity of singularities, the transverse stiffness of the boards E_{90} is not neglected in the calculations, even if the boards are not edge-glued. It is essential for obtaining the necessary tensile stresses σ_{90} perpendicular to the grain as shown in Fig. 2. In most cases, the gap between the boards is not located directly at the edge, and the boards are notched. Therefore, from a mesoscopic point of view, considering the transverse stiffness E_{90} makes sense.

Fig. 4 qualitatively illustrates the difference in the occurring stresses between the regular region and regions with singularities, caused by normal forces n_x and n_y. In the regular region, no transverse stresses $\sigma_{90,k}$ occur, while in the detailed region, transverse stresses $\sigma_{90,k}$ are present. For clarity, the magnitude of $\sigma_{90,k}$ is shown exaggerated. Also in Fig. 4 the shear stress τ_{xy} distribution induced by n_{xy} (see Eq. (20)) and vice versa τ_{yx} induced by n_{yx} is shown.

2.4. Experimental campaigns used for validation

To validate our approach for evaluating stress concentrations at the corners of openings in CLT shear members, we utilized two recently made experimental campaigns.

Casagrande et al. [5] conducted experimental tests on symmetric CLT shear walls made of spruce, examining six different wall configurations, with one specimen per configuration, to characterize their mechanical behavior. Similarly, Mestar et al. [4] investigated the kinematic modes of symmetric CLT walls through experiments on five distinct geometrical configurations, also using one specimen per configuration.

3. Numerical models of the experiments

This chapter presents the numerical models of the experiments. First, the geometrical and material properties are defined. Second, the mechanical behavior of the hold-downs is discussed. To give a proper insight into the models, one numerical model (M2) is presented in detail, including its support and load conditions as well as representative results.

3.1. Geometry and dimensions

The geometries of the walls from the two considered test series and thus the basis for our numerical models are summarized in Table 1. The specified geometric dimensions are defined in Fig. 5. Each wall is defined by its length ℓ and height h, while each opening is characterized by its length ℓ_o and height h_o. The height of the lintel is defined by h_ℓ. The horizontal shear load F acts on the upper side of the wall. The positions of the horizontal supports (HS) and hold-downs (HD) are also indicated for each configuration.

3.2. Material properties

In Table 2 the layup and the elastic material properties for each specimen are given. The number N of the layers, the total thickness t of the walls, and the width w of the individual boards are also given. In the definition of the layups, "v" stands for vertical alignment and "h" for horizontal alignment. The elastic properties for C1–C6 are taken from the European Technical Approval (ETA) [25] which is referenced in [5]. The properties from M1–M5 are based on the information which

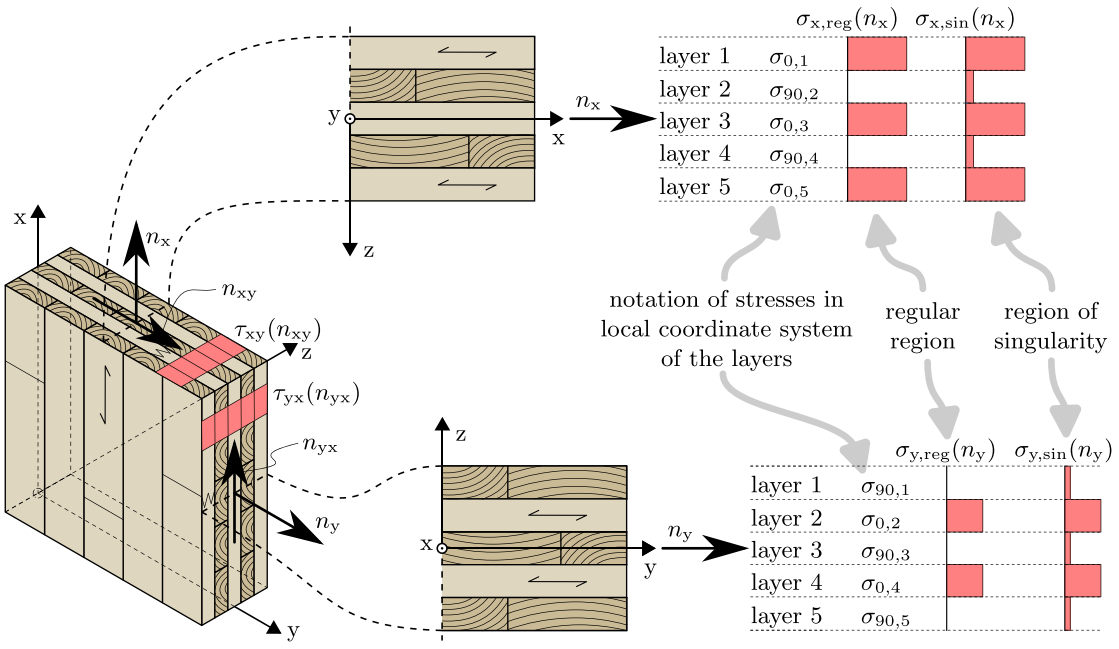

Fig. 4. Occurring stresses in CLT shear members for the regular and the detailed regions.

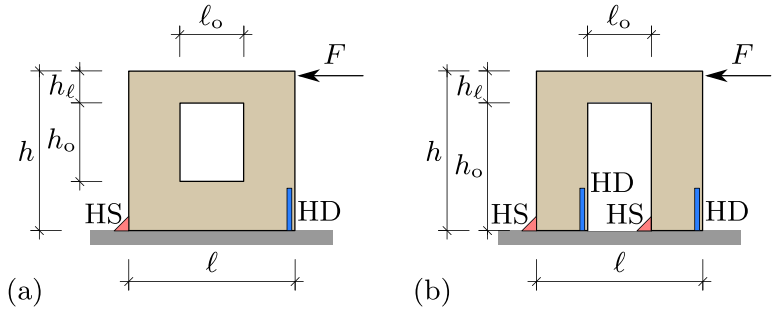

Fig. 5. Properties for the symmetric shear-walls with: (a) windows, (b) doors.

is given in Mestar et al. [4]. On the basis of those material properties, the stiffness properties for the simulation, for both detailed and regular regions, were calculated according to Eqs. (14) to (16) and are given in Table 3.

The critical energy release rates, $G_{I,c}$ and $G_{II,c}$, for Mode I and Mode II, respectively, are not standardized for spruce, unlike stiffness or strength, for which grading classes are available in material codes.

In the early 1990s, Larsen and Gustafsson [26] presented the results of a collaborative testing project on the fracture energy of softwood loaded in tension perpendicular to the grain. A total of eleven institutions participated, generating a substantial dataset. Based on this, a regression formula was developed to estimate the fracture energy for Mode I as a function of the mean density. For example, assuming a mean density of $\rho_{mean} = 420$ kg/m^3 for C24 solid wood according to EN 338 [27], the resulting fracture energy is:

$$G_{I,c} = 1.04\rho_{mean} - 146\,\text{N/m} = 291\,\text{N/m}\,. \tag{21}$$

Eq. (21) was also included in the background document [28] that supported the development of the Eurocode 5 design equation for notched beams. In a related study, Riberholt et al. [29] conducted an extensive experimental investigation on notched beams made of coniferous solid wood and glued laminated timber. By testing 101 specimens, they determined an average fracture energy of $G_{I,c} = 298$ N/m. Jockwer [30] analyzed various experimental results from the literature regarding the fracture energy $G_{I,c}$, determining a mean value of $G_{I,c,mean} = 306$ N/m. Therefore, for Mode I, we adopted a critical energy release rate of $G_{I,c} = 300$ N/m in our verification. This value has also been used in previous simulations [11,14,31].

Jockwer [30] also examined test results for the fracture energy $G_{II,c}$ and noted the increased complexity of its experimental determination, leading to higher variability. Previous simulations have employed different values for $G_{II,c,mean}$, typically ranging from 1050 N/m to 1150 N/m [11,14,31]. According to Jockwer [30], other sources report mean values ranging from 900 N/m to 1000 N/m. Riberholt et al. [29] also conducted tests on Mode II fracture and determined a mean value of $G_{II,c} = 945$ N/m. In our simulations for Mode II, we adopted a conservative value of $G_{II,c} = 900$ N/m, which is three times higher than $G_{I,c}$.

In general, in a mixed-mode scenario, Mode I is more critical and has a greater influence on the fracture load. This is reflected in the fracture criterion Eq. (11) and also makes sense from a safety-related perspective due to the lower fracture energy of spruce in Mode I.

3.3. Hold downs

In the simulations, the stiffness of the hold-downs was considered using the load–deformation curves presented in Fig. 6. The curve corresponding to the hold-downs WHT620 was taken from Casagrande et al. [5], where component tests were also conducted. In that study, the hold-downs were fully nailed using 55 nails of 4 × 60 mm. Similarly, in Mestar et al. [4] for M5, hold-downs WHT620 with 55 nails of 4 × 60 mm were used, allowing the same load–deformation curve to

Table 1
Overview of the considered experimental and in this work simulated shear wall configurations (dimensions definitions in Fig. 5).

Source	ID	Layout	Opening	ℓ m	h m	h_ℓ m	ℓ_o m	h_o m	HD type
[4]	M1		Door	1.95	2.60	0.60	0.75	2.00	WHT440
[4]	M2		Door	1.95	2.60	0.60	0.75	2.00	WHT440
[4]	M3		Window	1.90	2.60	0.40	0.70	1.10	WHT440
[4]	M4		Window	1.90	2.60	0.40	0.70	1.10	WHT440
[4]	M5		Door	2.30	2.60	0.30	1.00	2.30	WHT620
[5]	C1		Door	3.30	2.38	0.34	0.60	2.04	WHT620
[5]	C2		Door	3.30	2.38	0.34	0.90	2.04	WHT620
[5]	C3		Window	3.30	2.38	0.34	0.90	1.70	WHT620
[5]	C4		Door	3.90	2.38	0.51	1.50	1.87	WHT620
[5]	C5		Door	3.90	2.38	0.34	1.50	2.04	WHT620
[5]	C6		Window	3.90	2.38	0.34	1.50	1.70	WHT620

Table 2
Material properties of shear walls.

ID	Grade	t mm	N	Layup	w mm	E_0 N/mm^2	E_{90} N/mm^2	G_{090} N/mm^2
M1–M5	C24	85	5	17v-17h-17v-17h-17v	150	11 000	370	690
C1, C4	C24	90	3	30v-30h-30v	170	11 500	370	690
C2, C3, C5, C6	C24	100	5	20v-20h-20v20h-20v	170	11 500	370	690

Table 3
Stiffness properties for the regular and detailed regions of the simulated shear walls.

ID	$S_{xx,reg}$ kN/m	$S_{yy,reg}$ kN/m	$S_{xy,reg}$ kN/m	$S_{xx,sin}$ kN/m	$S_{yy,sin}$ kN/m	$S_{xy,sin}$ kN/m
M1–M5	561 000	374 000	49 490	573 580	392 870	49 490
C1, C4	690 000	345 000	44 681	701 100	367 200	44 681
C2, C3, C5, C6	690 000	460 000	57 806	704 800	482 200	57 806

be applied. For the other experimental setups M1–M4, hold-downs WHT440 with 30 nails of 4 × 60 mm were used. For them, a bi-linear load–deformation curve was derived from experimental results presented in Casagrande et al. [32].

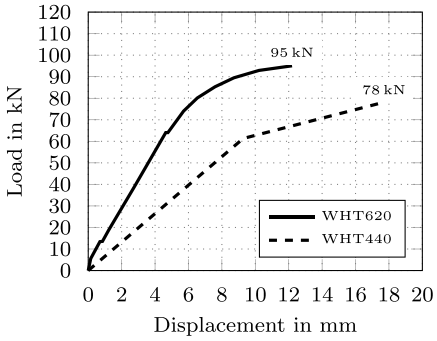

Fig. 6. In the simulation used load–deformation curves for the hold-downs WHT440 (according to [32]) and WHT620 (according to [5]).

3.4. Meshing

In order to capture stress distributions required for further evaluation accurately, the mesh density of the used 2D rectangular elements must be sufficiently fine in the vicinity of stress concentrations. In Appendix A.1, a mesh study using a notched beam, which represents one layer of a CLT member, is shown. Based on the findings, we recommend using a circular mesh refinement with a radius $r_{FE,refined}$ and a minimal inner mesh size defined as follows:

$$\ell_{FE,i} = \frac{x_0}{300}, \tag{22}$$

where $x_0 = 15$ mm, resulting in an inner mesh size of 0.05 mm used in our simulations. In all simulations, $r_{FE,refined}$ was set to 20 cm. The mesh size $\ell_{FE,reg}$ in regular regions without singularities depends on the geometric shape and size of the specimen and ranges from 6 cm to 8 cm. It can be stated that the mesh size of the regular regions has a rather small impact on the load-bearing predictions compared to the mesh refinement in the corners.

3.5. Dealing with round corners

The experimental documentations do not clearly indicate whether every opening in the CLT walls is rounded at the corners. Therefore, every corner of the openings in the simulations was modeled without

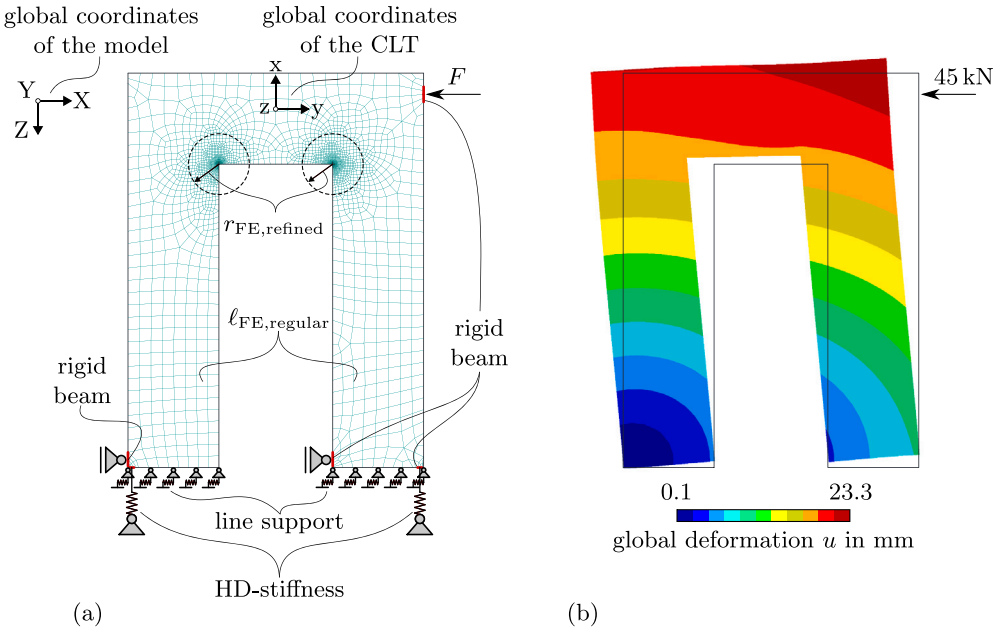

Fig. 7. Example of the finite element model M2: (a) model with support and mesh definitions, (b) global deformation u for a horizontal load $F = 45\,\mathrm{kN}$.

rounding. But there are also other reasons for neglecting rounding in the simulations.

In the fabrication of CLT elements, openings are mainly obtained using full CNC-machines with finger milling cutters with diameters of 20 mm to 40 mm, resulting in rounding radii of 10 mm to 20 mm. Due to the strong anisotropy of wood, such small roundings do not change the strain and stress distribution in such a way that the overall load-bearing capacity is affected significantly. Additionally, the execution quality of roundings can be very variable due to unsharp cutters, etc., making a detailed simulation of roundings much more difficult. Beside that, some practitioners are cutting openings in CLT elements without roundings. Our approach aims to be universal and straightforward for engineers in practice. Therefore, neglecting roundings in the simulations is also necessary from this perspective.

Based on the simulation results in Section 4, it is recognizable that neglecting rounded corners has no significant impact.

3.6. Prediction of the load-bearing capacity

To predict the load-bearing capacity of each numerical model, two main types of failure are investigated. Either the failure of a hold-down or the failure of a corner limits the load-bearing capacity of a shear wall. That was also noted in Mestar et al. [4] and Casagrande et al. [5]. The regular regions are not accounted for in the prediction of failure loads, as they did not govern the failure in the experiments.

3.7. Example of the numerical model for M2

The numerical models of each experiment consist of the same elementary components. First, the geometry of the wall with openings is discretized using 2D finite elements. Then, three different support conditions are required to capture a realistic deformation behavior of the CLT walls. The hold-downs, with mechanical behavior according to Fig. 6 can only transmit vertical tensile forces, while the compliance-less horizontal point supports only prevent horizontal displacement. The vertical support is modeled as a line support with full vertical bearing capacity in compression, no vertical bearing capacity in tension, and horizontal bearing capacity due to friction. To model frictional resistance, horizontal springs were added along the line support at the bottom of the wall. These springs represent the effect of contact friction, defined by a stiffness proportional to the normal force, representing a friction coefficient of 0.25. For a more realistic load introduction into the CLT walls, so-called rigid beams are used at the horizontal point supports and at the point of application of the horizontal load F.

For illustration, and in the representation of all experiments, the numerical model of experiment M2 with all the elementary components is shown in Fig. 7a. As an example, the global deformation obtained under a horizontal load $F = 45\,\mathrm{kN}$ is shown in Fig. 7b. It is visible that the right part is completely lifted off, and the remaining vertical contact of the wall element is concentrated on the left corner of the entire wall element. By looking at the global deformation field u, it can be expected that the right corner of the door opening is the critical one, because this corner opens under the current deformation, and critical tensile stresses perpendicular to the grain are induced. To consolidate this assumption, the distribution of the internal forces has to be analyzed. Critical corners are those with tensile normal forces.

In Fig. 8, the corresponding distribution fields of the internal forces n_x, n_y, and n_{xy} are shown. For the normal forces n_x and n_y, only the critical positive values (tensile normal forces) are shown. It should be mentioned, that for the sake of clarity, the ranges of the legend in Fig. 8 have been optimized. The minima and maxima values are significantly higher at the corners. As expected, the critical concentration of tensile normal forces is in the right corner of the door opening. With this knowledge, this corner, and, the stress concentration occurring there, has to be further analyzed.

As previously shown in Fig. 2, we define for each layer a potential crack surface originating from a corner. Based on this, the mean forces can be read out, and using Eqs. (18) to (20), the corresponding mean stresses can be calculated. In our example of M2, which is a five-layered CLT wall, two potential crack formations are identified (see Fig. 9). The first is a vertical crack formation in the vertical layers (two cover layers 1 and 5 and the middle layer 3). The second is a horizontal crack formation in the two horizontal inner layers 2 and 4. For the vertical crack formation in the vertical layers, the normal force n_y is responsible for the tensile stresses σ_{90}, which are acting perpendicular to the grain direction of the boards. For the horizontal crack formation in the horizontal inner layers, n_x is responsible for the local tensile stresses σ_{90}. The shear stresses σ_{090} for both crack formations are obtained from the shear force n_{xy}.

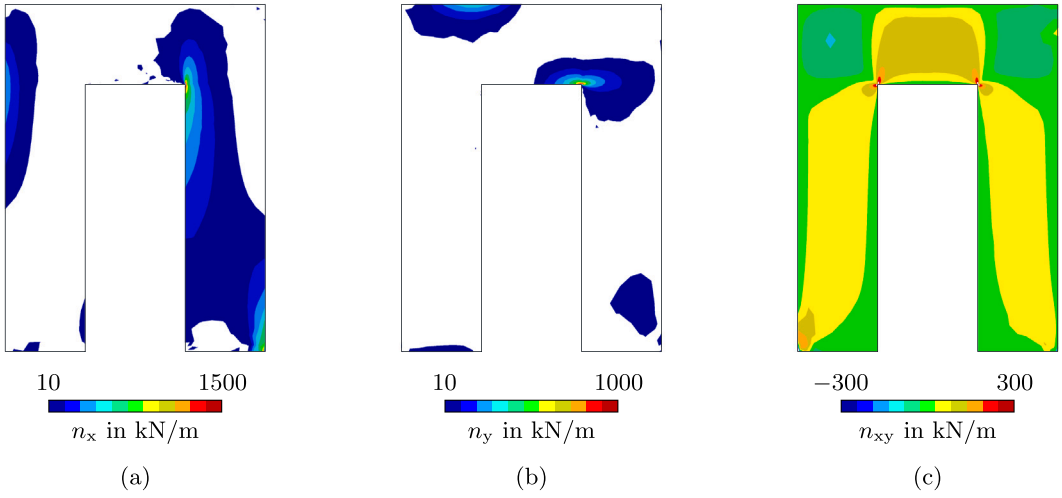

Fig. 8. Internal force distribution for M2 with a horizontal load $F = 45\,\text{kN}$: (a) normal force n_x, (b) normal force n_y, (c) shear force n_{xy}.

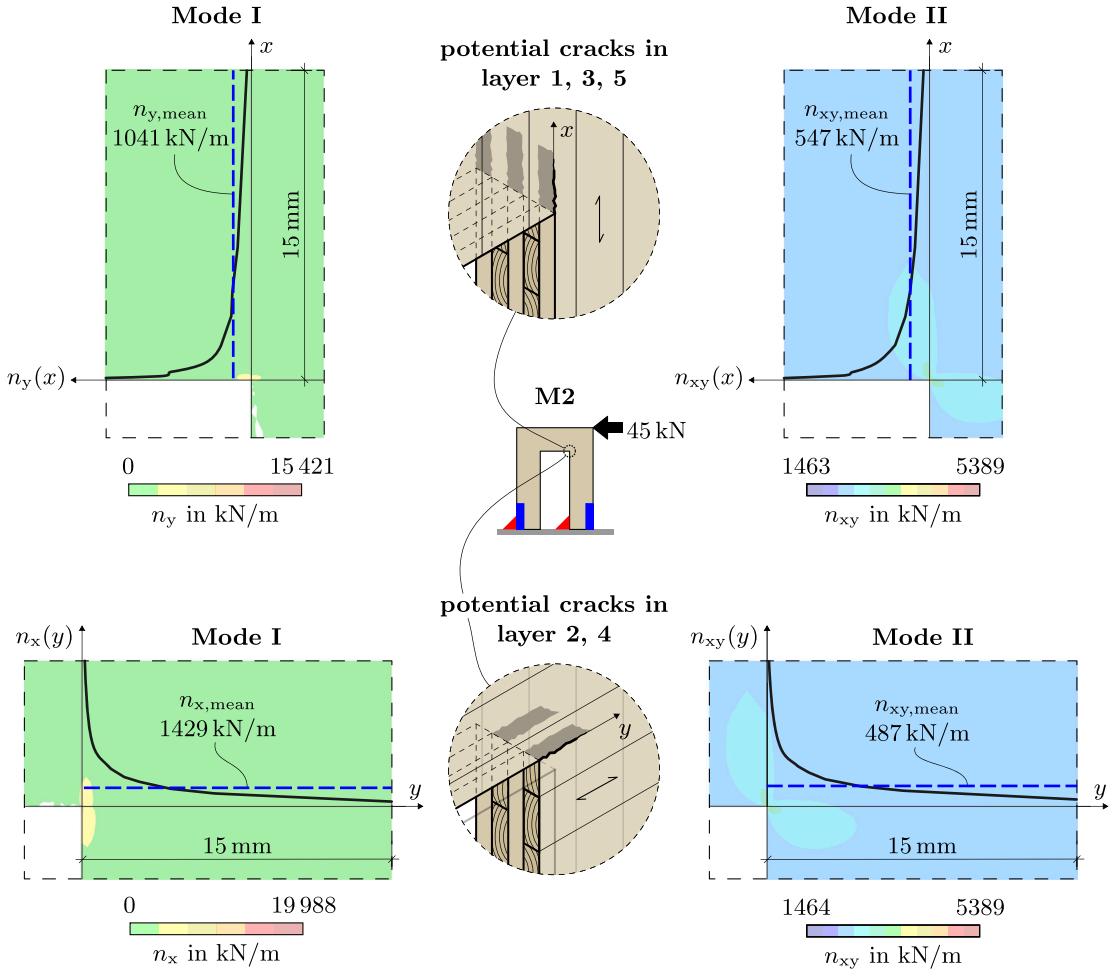

Fig. 9. Potential crack formations in wall M2 and the associated mean internal forces for calculating the mean stresses which are used to calculate the energy release rates.

4. Results & discussion

Overall, the numerical simulations of the specimens of both experimental campaigns show good accordance with regard to the load-bearing capacity and the deformation behavior. Also, the failure reasons, hold-down failure, and CLT failure can be distinguished in the simulation and showed a good agreement with the experimental results.

In the following, the results of the experiments and the numerical simulations are detailed presented and compared. After that, the applicability of the proposed approach is discussed.

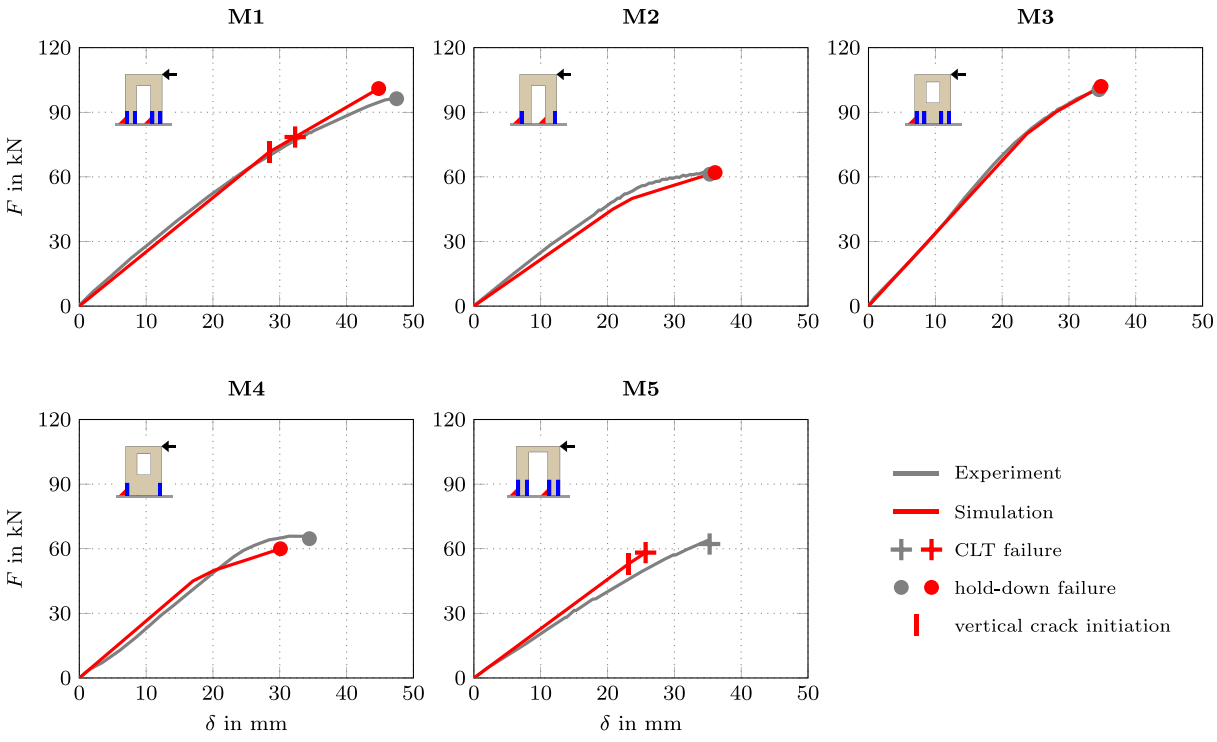

Fig. 10. Results of the experiments from Mestar et al. [4] and the corresponding simulations.

4.1. Results of the experiments and the simulations — comparison

The results of the numerical models and the results of the corresponding experiments are depicted in Fig. 10 for the experiments from Mestar et al. [4] and in Fig. 11 for the experiments from Casagrande et al. [5].

The following notation should be considered: The gray lines represent the experiments, while the red ones show our simulations. The failure modes are also specified, distinguishing between hold-down failure and CLT failure. Hold-down failure is represented by a filled circle, whereas full CLT failure is depicted with a cross. Full CLT failure occurs when cracking is obtained in every layer (see Eq. (13)). The so-called elastic limit, where at least one crack occurs in at least one layer (see Eq. (12)), is shown by a vertical line. In all simulations, when cracking is predicted, the first crack initiation occurs in the top layers, which in all cases are the vertical ones. For full CLT failure, and thus, crack initiation in all layers, the inner horizontal layers also show horizontal crack initiation. So, the symbolism corresponds to the crack direction: the vertical line shows vertical crack initiation in the vertical layers, and the cross represents full crack initiation, including vertical cracks in the vertical layers and horizontal cracks in the horizontal inner layers.

First, we discuss the results of the experiments from Mestar et al. [4] and the corresponding simulations. According to Mestar et al. [4], the ultimate failure of M1 occurred as a combination of CLT failure and hold-down failure. CLT failure was specified as wood tension failure, but it was unfortunately not further described. However, the simulation was capable of predicting the final bearing load which led to hold-down failure very well. Additionally, crack initiation at a slightly lower load level was predicted, which matches the explanations in Mestar et al. [4].

Specimen M2 failed due to clear hold-down failure, which was perfectly predicted by the simulation. Matching the experiments, also in the simulation, no previous crack initiation was predicted. The same applies to specimens M3 and M4. The implementation of the load–deformation curves for the hold-downs (Fig. 6) leads to nonlinear load–deformation curves for the walls, which fits very well with the experimental results.

Specimen M5 showed plain CLT failure in the lintel in the experiments. Mestar et al. [4] described the failure twofold: the lintel beam failed at the top left above the opening and in the right corner of the opening. The corresponding image of the failure of the right corner in Mestar et al. [4] confirmed our assumption of full CLT failure when every layer undergoes crack initiation. This failure type in the right corner and the corresponding failure load were predicted extremely well in the simulation.

Next, the results of the experiments from Casagrande et al. [5] and the corresponding simulations are discussed. According to Casagrande et al. [5], specimen C1 showed clear CLT failure in the right corner of the opening, with vertical cracks in the two vertical top layers and horizontal crack initiation in the horizontal inner layer. This behavior was also predicted in the simulation, resulting in a very good agreement with the experimental result.

Specimen C3 was reported in Casagrande et al. [5] to exhibit clear hold-down failure, with no cracks in the wood documented in the area of the corners. The corresponding simulation also predicted clear hold-down failure with no crack initiation.

CLT failure was also the reason for the failure of specimen C4. According to Casagrande et al. [5], the failure occurred on the upper side of the lintel, above the left corner of the opening, in a region without stress singularities. It was associated with finger-joint failure in the inner horizontal boards of the wall. However, Casagrande et al. [5] noted that the loading continued beyond potential initial cracks until ultimate failure was reached. This suggests the possibility that crack initiation may have started in the right corner, where a stress singularity exists, but it was not the cause of ultimate failure. In our simulation, only the right corner was investigated, resulting in an adequate prediction of the load-bearing capacity on the safe side. For further investigation, more details about that specimen during the experiment, such as video recordings of the test, would be required.

Specimens C2, C5, and C6 failed due to hold-down failure. The load level of the final hold-down failure was predicted very well in the simulations, as shown in Fig. 11. However, the simulations also

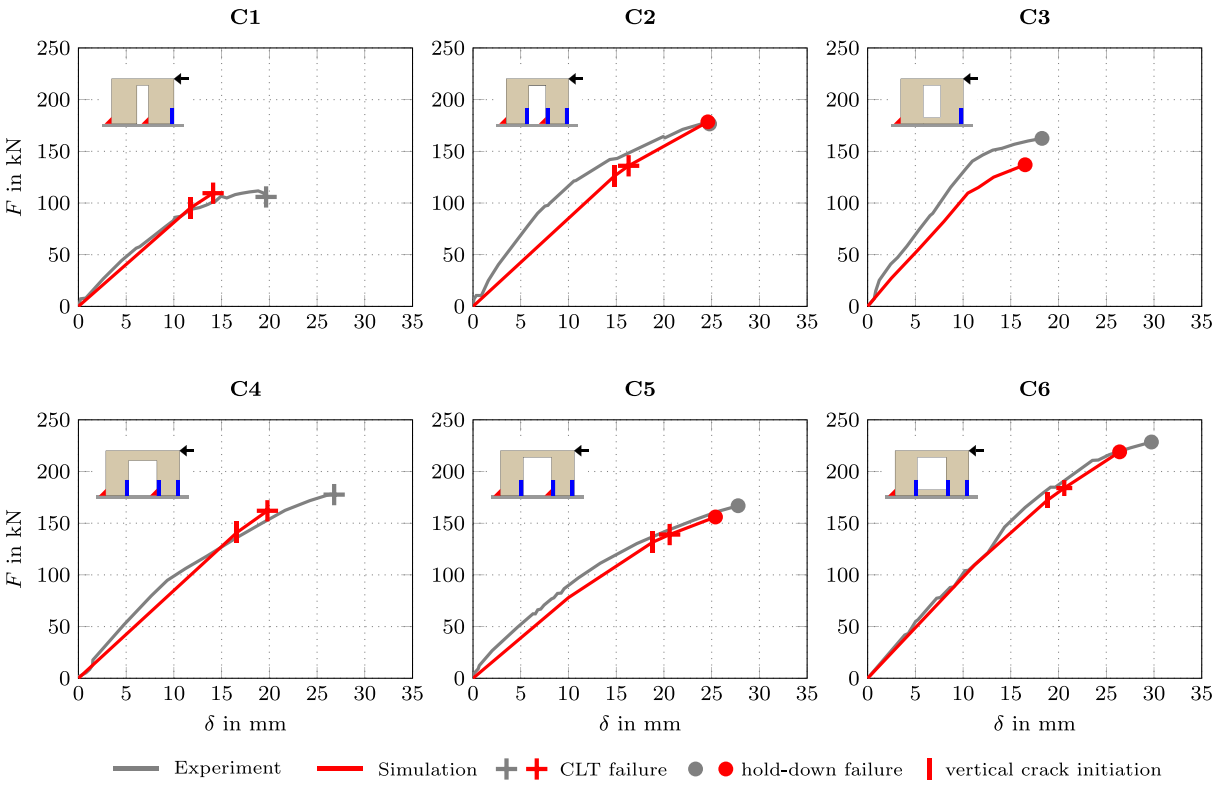

Fig. 11. Results of the experiments from Casagrande et al. [5] and the corresponding simulations.

Table 4
Comparison of maximum experimental loads F_{test} from Mestar et al. [4] and Casagrande et al. [5] with corresponding simulation predictions F_{sim} (relative devitation $\epsilon = \frac{F_{sim}-F_{test}}{F_{test}} \cdot 100\,\%$).

Source	ID	F_{test} kN	F_{sim} kN	ϵ %
[4]	M1	96	101	5.2
[4]	M2	61	62	1.6
[4]	M3	100	102	2.0
[4]	M4	65	60	−7.7
[4]	M5	62	58	−6.5
[5]	C1	112.8	109.5	−2.9
[5]	C2	176.5	178.5	1.1
[5]	C3	160.9	137.0	−14.9
[5]	C4	178.6	162.0	−9.3
[5]	C5	165.9	156.0	−6.0
[5]	C6	226.8	219.0	−3.4

predicted crack initiation and, finally, CLT failure at lower load levels. Due to the lack of detailed information about the behavior of the specimens during the experiment with increasing load, it is possible that small cracks did appear in the right corners but did not cause the final failure. As mentioned before, more details from the experiments would be helpful. Nevertheless, the predicted bearing loads for failure in the corners are on the safe side and not too conservative from an engineering point of view.

Table 4 compares the maximum loads F_{test} obtained from the experiments in Mestar et al. [4] and Casagrande et al. [5] with the numerically predicted failure loads F_{sim}, focusing on the failure mechanisms described in the referenced studies. The relative deviations ϵ indicate that the numerical models tend to be slightly conservative, with a maximum underestimation of −14.9 %. The maximum overestimation was relatively small, at 5.2 %.

4.2. Discussion

Two mechanical properties are essential for the prediction and design of CLT walls: the deformation behavior and the failure load level with the corresponding failure type. Our numerical models can describe both to a sufficient extent and with high efficiency.

The load–deformation curves from the simulations show overall good agreement with the experiments. This indicates that the stiffness definitions for the two main mechanical elements of each wall configuration, the CLT wall and the hold-downs, were appropriate. Classical laminate theory, as described in Section 2.3.1, is therefore perfectly qualified to describe the stiffness properties of CLT. Also, the implementation of the mechanical behavior of hold-downs with bilinear or experimentally determined load–deformation curves in a numerical simulation can be recommended. This allows the model to consider their impact on both the load–deformation behavior and also on the load-bearing capacity of a CLT shear wall very well.

Our proposed approach to predicting the load-bearing capacity of CLT walls based on the assessment of stress singularities at the corners of openings has, as expected, proven to be an approach that is on the safe side, but not too conservative. Although stress redistribution after the failure of a single layer (see Eq. (12)) is not considered, the second failure criterion (Eq. (13)) yields similar load-bearing capacities. This suggests that quasi-brittle failure modes are not significantly influenced by such redistribution effects and can be reliably predicted using the proposed failure criteria.

The precise rounding/finishing of the corners in openings probably does not have a major influence on the load-bearing capacity and, therefore, does not need to be taken into account in the numerical model.

4.3. Proposal for implementation in design standards

So far, we have used mean values of the critical energy release rates to define crack initiation. However, in design verification approaches,

characteristic values must be used for safety reasons, along with factors that account for material variability, environmental conditions, and load duration.

Therefore, based on the suggestions of Aicher et al. [33], who used stress intensity factors K, we recommend the following design criterion:

$$\sqrt{\frac{G_{\mathrm{I,d}}}{G_{\mathrm{I,c,d}}}} + \frac{G_{\mathrm{II,d}}}{G_{\mathrm{II,c,d}}} \leq 1.0 \ , \tag{23}$$

where $G_{\mathrm{I,c,d}}$ and $G_{\mathrm{II,c,d}}$ in Eq. (23) are the critical design energy release rates:

$$G_{\mathrm{I,c,d}} = k_{\mathrm{mod}} \frac{G_{\mathrm{I,c,k}}}{\gamma_{\mathrm{M}}}, \quad G_{\mathrm{II,c,d}} = k_{\mathrm{mod}} \frac{G_{\mathrm{II,c,k}}}{\gamma_{\mathrm{M}}} \ , \tag{24}$$

and $G_{\mathrm{I,d}}$ and $G_{\mathrm{II,d}}$ are the design energy release rates obtained from simulations under ultimate limit state (ULS) load combinations.

In Eq. (24), $G_{\mathrm{I,c,k}}$ and $G_{\mathrm{II,c,k}}$ are characteristic values of the critical energy release rates and can be found in the literature, such as in Jockwer [30]. The modification factor k_{mod}, which accounts for load duration and service class, as well as the partial material safety factor γ_{M}, are both specified in EC5 [24].

5. Conclusion & outlook

In this work, we have presented an engineering approach to predict the load-bearing capacities of CLT walls with openings. This approach is based on a linear elastic fracture mechanics assessment of stress fields in the vicinity of singularities. This is intended to establish a mechanically sound alternative to an arbitrary averaging of stresses in the vicinity of singularities or the exclusion of edge stresses in numerical analyses, both of which are common practice.

With our approach, the energy release rates G_{I} for Mode I and G_{II} for Mode II, occurring at sharp corners, can be calculated using the stress fields of a simple numerical 2D model, without the need of advanced finite elements. Based on this, we developed two failure criteria capable of predicting the load-bearing capacity of a corner in a CLT wall under in-plane shear loading.

To validate our proposed approach, we used experimental results from the literature and compared them with our numerical results obtained by finite element simulations. We modeled the CLT walls using 2D finite elements with stiffness properties calculated according to classical laminate theory. Additionally, the hold-downs were implemented in detail using load–deformation curves and corresponding failure definitions.

In conclusion, our procedure for predicting the load-bearing capacity of an entirely CLT shear wall with opening, while addressing the main failure mechanisms: hold-down failure and CLT failure in corners with stress singularities, using a relatively simple finite element simulation, is highly effective in depicting the experimental results.

The load-bearing capacity is assessed based on linear 2D finite element calculations. This is extremely efficient compared to advanced methods such as damage, plasticity or methods for describing discrete cracks. The proposed method for assessing stress singularities is not limited to RFEM 5 [20] and can be implemented in any finite element software that supports 2D modeling with linear elastic orthotropic material definitions. To apply the method reliably, the software should also support reasonable mesh refinement in regions near discontinuities (e.g., notches or corners). These requirements – 2D FE analysis, orthotropic elasticity, and mesh control – are typically met by most commercial finite element packages used in civil and structural engineering

With all these benefits, we recommend that the proposed approach be considered in the design process of CLT shear walls using finite element software and be considered in future design codes, making the use of finite element software more appealing to practitioners in timber engineering.

As an outlook for further investigation and potential application of the proposed approach, additional experimental results could be used. For example, further experimental data on shear walls with openings can be found in [6,34–36]. The proposed approach should also be able to predict the load-bearing capacity of CLT shear members with shapes other than walls with openings. A basis for validation of this assumption could be the experimental campaign of Aljuhmani et al. [18], who investigated openings in in-plane shear loads CLT panels made from Japanese cedar. Also, the results of Isoda et al. [9], who tested in-plane shear-loaded L-shaped and T-shaped CLT panels, also made from Japanese cedar, would be interesting for further validation. Future validation of the approach could also focus on 3D building-scale models, where interactions with floor diaphragms are considered.

CRediT authorship contribution statement

Markus Detter: Writing – original draft, Validation, Methodology, Formal analysis, Visualization, Software, Investigation, Conceptualization. **Georg Hochreiner:** Writing – review & editing, Methodology, Software, Conceptualization. **Josef Füssl:** Supervision, Funding acquisition, Writing – review & editing, Methodology, Conceptualization.

Declaration of competing interest

The authors declare that they have no known competing financial interests or personal relationships that could have appeared to influence the work reported in this paper.

Acknowledgments

The authors gratefully acknowledge the funding from the Austrian Research Promotion Agency (FFG) through the Collective Research Projects FO999903793 and FO999921467 in cooperation with the Austrian Timber Engineering Association (IHBV). This research was funded in whole or in part by the Austrian Science Fund (FWF) [START project Y1093-N30]. For open access purposes, the author has applied a CC BY public copyright license to any author accepted manuscript version arising from this submission. The authors acknowledge TU Wien Bibliothek for financial support through its Open Access Funding Programme.

Appendix. Sensitivity analysis

This appendix presents a parametric study evaluating the sensitivity of the proposed method to three key parameters: the mesh refinement near singularities, the length x_0, and the critical energy release rates $G_{\mathrm{I,c}}$ and $G_{\mathrm{II,c}}$.

First, in Appendix A.1, we provide recommendations for the required mesh refinement at the potential crack tip, as previously discussed in Section 3.4. Second, in Appendix A.2, we investigate the influence of the length x_0 and the mesh refinement radius on the total energy release rate. Finally, we assess the impact of the critical energy release rates on the results obtained using the fracture criterion defined in Eq. (11).

The basis for the parametric study is a notched cantilever beam, modeled in RFEM 5 [20], as shown in Fig. A.12.

A.1. Necessary mesh refinement

To investigate the impact of the type of FE mesh refinement on the total energy release rate $G = G_{\mathrm{I}} + G_{\mathrm{II}}$, two variants of mesh refinement were analyzed:

Variant 1: Circular mesh refinement with a variation of the inner FE mesh size $\ell_{\mathrm{FE,i}}$.

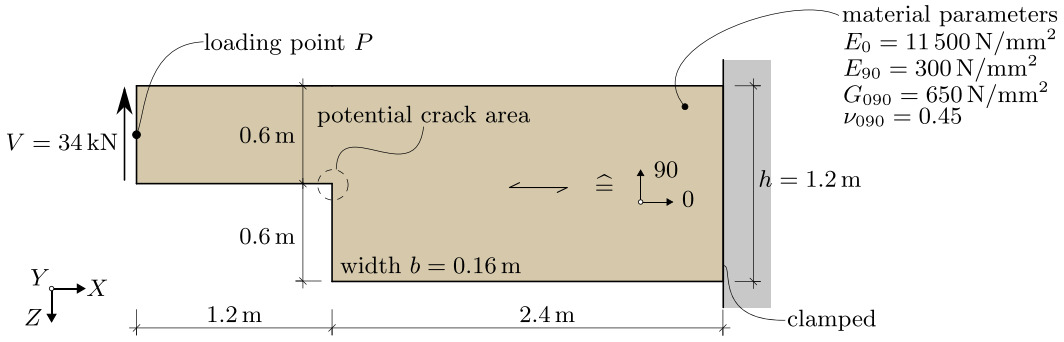

Fig. A.12. Geometry and material parameters of the notched cantilever beam.

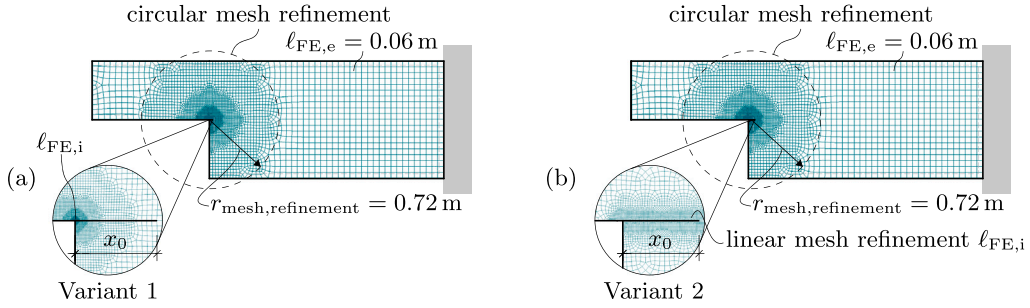

Fig. A.13. Mesh variants: (a) variant 1, (b) variant 2.

Variant 2: Circular mesh refinement with a constant inner FE mesh size $\ell_{\mathrm{FE,i}} = 7.5\,\mathrm{mm}$ and additional varied linear mesh refinement across the length x_0 using $\ell_{\mathrm{FE,i}}$.

These two types of FE mesh refinement were applied to the model (see Fig. A.13), with a refinement radius defined as $r_{\mathrm{mesh,refinement}} = 0.72\,\mathrm{m}$. The global setting for all FE elements outside the circular mesh refinement area is $\ell_{\mathrm{FE,e}} = 0.06\,\mathrm{m}$.

The internal FE mesh size $\ell_{\mathrm{FE,i}}$ in the vicinity of singularities is of particular interest and is varied in variant 1 and in variant 2 (only linear mesh refinement) for comparison calculations as follows:

$$\ell_{\mathrm{FE,i}} = \frac{x_0}{a} \tag{A.1}$$

where $a > 0$ represents a factor for discretization. Thus, the internal FE mesh size is expressed solely by the length x_0 and the factor a. The length x_0 was defined with 15 mm.

Therefore, for each variant, eleven models were calculated with the factor a varying from 1 to 960. The energy release rates G_{I} and G_{II} were calculated according to Eqs. (9) and (10), and the results are presented in Fig. A.14. Two conclusions can be drawn from this figure:

1. There is no significant difference between the two variants of FE mesh refinement.
2. Regardless of the variant of FE mesh refinement used, it is observed that the total energy release rate converges relatively quickly. Beyond a factor of $a = 300$, the results change only marginally.

For our calculations in this paper, variant 1 with factor $a_{\mathrm{min}} = 300$ is used (see Eq. (22)).

A.2. Influence of x_0 and mesh refinement radius

In the next step, we investigate the influence of the length x_0 and the mesh refinement radius $r_{\mathrm{r,mesh,refinement}}$ on the total energy release rate $G_{\mathrm{I}} + G_{\mathrm{II}}$. To this end, x_0 was varied between 10 mm to 30 mm (10 mm, 15 mm, 20 mm and 30 mm). All simulations were conducted using two

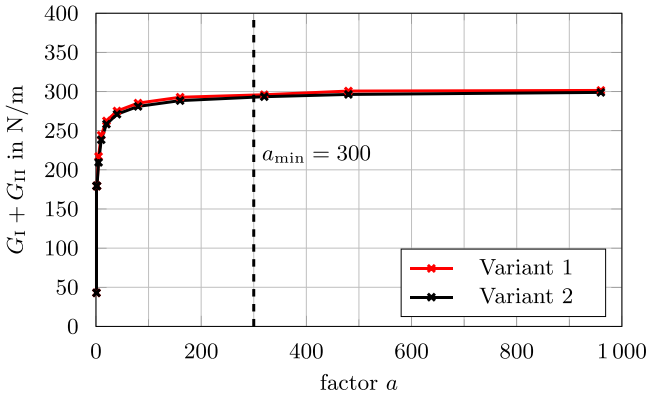

Fig. A.14. Comparison of variant 1 and variant 2 regarding the total energy release rate $G_{\mathrm{I}} + G_{\mathrm{II}}$.

values for $r_{\mathrm{r,mesh,refinement}}$: 72 cm and 20 cm. The mesh size was adjusted according to Eq. (A.1), based on $x_0 = 15\,\mathrm{mm}$.

The results are presented in Fig. A.15. It is evident that the total energy release rate converges relatively quickly. Changing the radius of the mesh refinement leads to only a minimal variation in the total energy release rate – approximately 5 N/m at $a = 300$. In contrast, varying x_0 (while keeping the refinement radius constant) results in a slightly larger difference of about 23 N/m at the same value for a. The chosen value of $x_0 = 15\,\mathrm{mm}$ therefore lies in the middle of the examined range and represents a reasonable balance.

It is also worth noting that the variation in total energy release rate remains relatively small, even though the mean stresses $\sigma_{90,\mathrm{mean}}$ and $\tau_{090,\mathrm{mean}}$ enter quadratically into the calculation of G_{I} and G_{II} (see Eqs. (9) and (10)). This indicates that the sensitivity to changes in x_0 and the mesh refinement radius is rather low. Overall, the results demonstrate that the proposed method is robust with respect to these parameter choices.

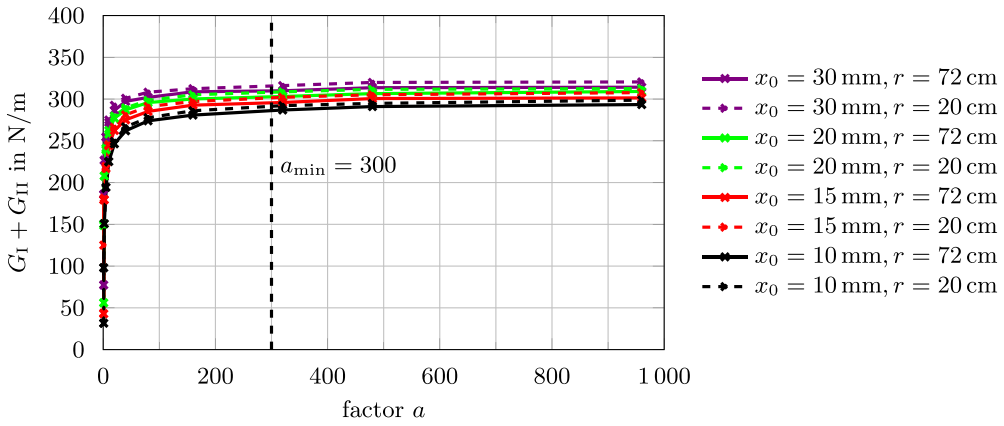

Fig. A.15. Influence of x_0 and $r_{r,mesh,refinement}$ (Variant 1) on the total energy release rate $G_I + G_{II}$ for different values of x_0 and mesh refinement radius.

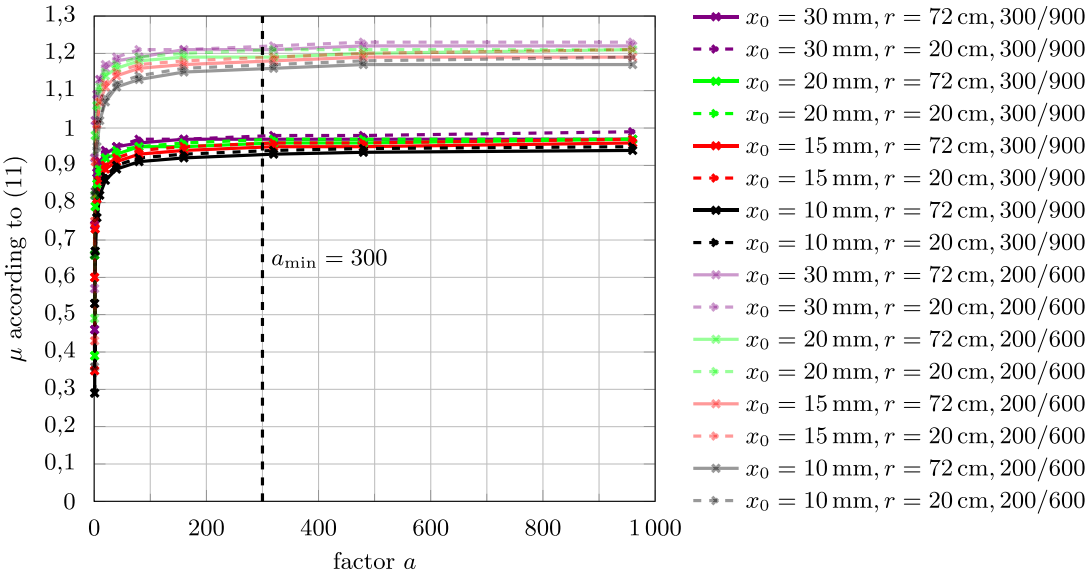

Fig. A.16. Influence of x_0, $r_{r,mesh,refinement}$ (Variant 1), and the critical energy release rates $G_{I,c}$ and $G_{II,c}$ on the fracture prediction according to Eq. (11).

A.3. Influence of the critical energy release rates on the results

Finally, the influence of the critical energy release rates $G_{I,c}$ and $G_{II,c}$ on the results obtained using the fracture criterion (see Eq. (11)) is examined. For this purpose, two sets of fracture energy values were used: $G_{I,c} = 300\,N/m$ and $G_{II,c} = 900\,N/m$ is the first case, and $G_{I,c} = 200\,N/m$ and $G_{II,c} = 600\,N/m$ is the second.

It is clearly evident in Fig. A.16, that the critical energy release rates have a dominant influence on the prediction of whether fracture occurs. When the lower values for $G_{I,c}$ and $G_{II,c}$ are applied, the utilization factor increases in a range of 0.23 to 0.24 at $a = 300$. So the impact of the critical energy release rates is significantly higher than the variations caused by changes in x_0 or the mesh refinement radius.

Data availability

Data will be made available on request.

References

[1] Sandoli A, D'Ambra C, Ceraldi C, Calderoni B, Prota A. Sustainable cross-laminated timber structures in a seismic area: Overview and future trends. Appl Sci 2021;11(5):2078. http://dx.doi.org/10.3390/app11052078, Publisher: MDPI AG.

[2] Casagrande D, Fanti R, Greco M, Gavric I, Polastri A. On the distribution of internal forces in single-storey CLT symmetric shear-walls with openings. Struct 2021;33:4718–42. http://dx.doi.org/10.1016/j.istruc.2021.06.084.

[3] Izzi M, Casagrande D, Bezzi S, Pasca D, Follesa M, Tomasi R. Seismic behaviour of cross-laminated timber structures: A state-of-the-art review. Eng Struct 2018;170:42–52. http://dx.doi.org/10.1016/j.engstruct.2018.05.060, Publisher: Elsevier BV.

[4] Mestar M, Doudak G, Polastri A, Casagrande D. Investigating the kinematic modes of CLT shear-walls with openings. Eng Struct 2021;228:111475. http://dx.doi.org/10.1016/j.engstruct.2020.111475.

[5] Casagrande D, Fanti R, Doudak G, Polastri A. Experimental and numerical study on the mechanical behaviour of CLT shearwalls with openings. Constr Build Mater 2021;298:123858. http://dx.doi.org/10.1016/j.conbuildmat.2021.123858.

[6] Dujic B, Klobcar S, Zarnic R. Influence of openings on shear capacity of wooden walls. In: Proceedings of the CIB-W18 meeting 40, 40-15-6. Bled, Slovenia; 2007.

[7] Shahnewaz I, Tannert T, Shahria Alam M, Popovski M. In-plane stiffness of cross-laminated timber panels with openings. Struct Eng Int 2017;27(2):217–23. http://dx.doi.org/10.2749/101686617X14881932436131.

[8] Sciomenta M. Fracture analysis of cross laminated timber shear-walls with openings. In: World conference on timber engineering. WCTE 2023, Oslo, Norway: World Conference on Timber Engineering (WCTE 2023); 2023, p. 2826–33. http://dx.doi.org/10.52202/069179-0370.

[9] Isoda H, Namba T, Kitamori A, Mori T, Miyake T, Nakagawa T, Tesfamariam S. Experimental behavior of L-shaped and T-shaped cross-laminated timber to evaluate shear walls with openings. J Struct Eng 2023;149(5). http://dx.doi.org/10.1061/JSENDH.STENG-11474.

[10] D'Arenzo G. An elastic model for the prediction of the lateral response of cross-laminated timber shear walls with openings. Eng Struct 2023;274:115055. http://dx.doi.org/10.1016/j.engstruct.2022.115055.
[11] Aicher S, Gustafsson PJ, Haller P, Petersson H. Fracture mechanics models for strength analysis of timber beams with a hole or a notch: A report of RILEM TC-133. TVSM-7000, Division of Structural Mechanics, LTH; 2002, number TVSM-7134.
[12] Irwin GR. Analysis of stresses and strains near the end of a crack traversing a plate. J Appl Mech 1957;24(3):361–4. http://dx.doi.org/10.1115/1.4011547.
[13] Serrano E, Gustafsson PJ. Fracture mechanics in timber engineering – Strength analyses of components and joints. Mater Struct 2007;40(1):87–96. http://dx.doi.org/10.1617/s11527-006-9121-0.
[14] Serrano E. Rational modelling and design in timber engineering applications using fracture mechanics. In: Eberhardsteiner J, Winter W, Fadai A, Pöll M, editors. WCTE 2016 e-book : Containing all full papers submitted to the world conference on timber engineering (WCTE 2016), August 22-25, 2016, vienna, Austria. 2016.
[15] Thelandersson S, Larsen HJ, editors. Timber engineering. John Wiley & Sons Ltd; 2003.
[16] Serrano E, Jockwer R, Danielsson H. Beams with notches or slits – Extensions of the Gustafsson approach. In: International network on timber engineering research - INTER. Bad Aibling, Germany; 2022.
[17] Wu EM. Application of fracture mechanics to anisotropic plates. J Appl Mech 1967;34(4):967–74. http://dx.doi.org/10.1115/1.3607864.
[18] Aljuhmani AG, Alwashali H, Ogasawara A, Atsuzawa E, Maeda M, Seki M. Experimental investigation on the effect of openings on the in-plane shear strength and stiffness of cross-laminated timber panels. Eng Struct 2022;254:113786. http://dx.doi.org/10.1016/j.engstruct.2021.113786.
[19] Gschwendtner S. Numerische Berechnung von Durchbrüchen in Brettsperrholz-Wandelementen. Diplomarbeit, Universität Innsbruck; 2022, in German.
[20] Dlubal Software GmbH. RFEM 5, version 5.32. URL: https://www.dlubal.com.
[21] Jones RM. Mechanics of composite materials. 2nd ed.. Philadelphia, Pa. [u.a.]: Taylor & Francis; 1999.
[22] Wallner-Novak M, Augustin M, Koppelhuber J, Pock K. Bemessung Brettsperrholz Band II – Anwendungsfälle. Wien: ProHolz Austria; 2018, in German.
[23] Bogensperger T, Silly G. Zweiachsige Lastabtragung von Brettsperrholzplatten. Bautechnik 2014;91(10):742–52. http://dx.doi.org/10.1002/bate.201300085, in German.
[24] ÖNORM B 1995-1-1:2019-06-01: Eurocode 5: Bemessung und Konstruktion von Holzbauten – Teil 1-1: Allgemeines – Allgemeine Regeln und Regeln für den Hochbau – Nationale Festlegungen, nationale Erläuterungen und nationale Ergänzungen zur ÖNORM EN 1995-1-1. Vienna: Austrian Standards, in German; 2019.
[25] European technical assessment – ETA 12/0362 – Solid wood slab elements to be used as structural elements in buildings. Expoo, Finland: Eurofins Expert Services; 2020.
[26] Larsen HJ, Gustafsson PJ. The fracture energy of wood in tension perpendicular to the grain – Results from a joint testing project. In: Proceedings of the CIB-W18 meeting 23, CIB-W18A/23-19-2. Lisbon, Portugal; 1990.
[27] ÖNORM EN 338:2016-06-01: Bauholz für tragende Zwecke – Festigkeitsklassen. Vienna: Austrian Standards, in German; 2016.
[28] Larsen HJ, Riberholt H, Gustafsson PJ. Annex to paper CIB-W18/25-102-1 EUROCODE 5 – Design of notched beams. In: Proceedings of the CIB-W18 meeting 25, 25-102-1A. Åhus, Sweden; 1992.
[29] Riberholt H, Enqvist B, Gustafsson P-J, Jensen RB. Timber beams notched at the support. TVSM-7000 TVSM-7071, Lund: Division of Structural Mechanics, LTH; 1992.
[30] Jockwer R. Structural behaviour of glued laminated timber beams with unreinforced and reinforced notches [Ph.D. thesis], ETH Zurich; 2014, http://dx.doi.org/10.3929/ETHZ-A-010171641.
[31] Danielsson H, Gustafsson PJ. A probabilistic fracture mechanics method and strength analysis of glulam beams with holes. Eur J Wood Wood Prod 2011;69(3):407–19. http://dx.doi.org/10.1007/s00107-010-0475-1.
[32] Casagrande D, Polastri A, Sartori T, Loss C, Chiodega M. Experimental tests for mechanical characterization of timber buildings connections. In: Eberhardsteiner J, Winter W, Fadai A, Pöll M, editors. WCTE 2016 e-book : Containing all full papers submitted to the world conference on timber engineering (WCTE 2016), August 22-25, 2016, vienna, Austria. 2016.
[33] Aicher S, Schmidt J, Brunhold S. Design of timber beams with holes by means of fracture mechanics. In: Proceedings of the CIB-W18 meeting 28, 28-19-4. Copenhagen, Denmark; 1995.
[34] Flatscher G, Bratulic K, Schickhofer G. Experimental tests on cross-laminated timber joints and walls. Proc Inst Civ Eng - Struct Build 2015;168(11):868–77. http://dx.doi.org/10.1680/stbu.13.00085.
[35] Araki Y, Nakashima S, Nakajima S, Yamaguchi Y. Study on the opening reduction coefficient of CLT panel with opening. AIJ J Technol Des 2018;24(56):147–52. http://dx.doi.org/10.3130/aijt.24.147, in Japanese.
[36] Awad V, Giresini L, Koshihara M, Puppio ML, Sassu M. Experimental analyses and numerical models of CLT shear walls under cyclic loading. In: Concu G, editor. Wood in civil engineering. InTech; 2017, http://dx.doi.org/10.5772/65024.